OPEN ACCESS

INSULATION DETECTION OF ELECTRICAL EQUIPMENT IN POWER SYSTEM BASED ON PHOTOACOUSTIC SPECTROSCOPY TECHNOLOGY

Xiaowei Zhang[1,], Yufeng Chang[1], Mingdong Zhu*
[1]Xuchang Vocational Technical College, Xuchang 461000, China

Abstract - Traditional insulation detection technologies for power equipment struggle to accurately capture trace characteristic gas signals of early insulation degradation and are hardly adaptable to the complex on-site operating conditions of substations. Based on photoacoustic spectroscopy (PAS) technology, this study constructs a quantitative detection model incorporating temperature and pressure corrections. It optimizes the sample pretreatment process and hardware parameters. By combining laboratory-based performance verification and on-site equipment adaptability tests, a complete insulation detection technology system for power equipment is established. The study focuses on three types of core equipment: 220 kV Gas Insulated Switchgear (GIS), 110kV transformers, and 35kV cross-linked polyethylene (XLPE) cables. Targeted sample processing schemes are designed. A 316L stainless steel photoacoustic cell and a distributed feedback (DFB) tunable semiconductor laser light source with a wavelength range of 1.5-11 μm are adopted. The signals are processed through 50Hz notch filtering and db4 wavelet filtering. Synchronous detection of multi-component gases is achieved by combining multi-wavelength switching and signal decoupling. The results show that the detection limit of this technology for SO_2F_2 in GIS equipment reaches 0.035 μL/L. The detection errors of the three types of on-site equipment do not exceed 3.8%, which is 1.4-2.2 percentage points lower than that of gas chromatography. Within the pressure range of 0.4-0.6 MPa in the GIS gas chamber, the detection deviation is stably maintained between 1.2% and 1.9%. The anti-interference ability and response speed scores reach 85 and 90 respectively, which are significantly better than those of infrared spectroscopy. The technology maturity score is 72, and the relative application cost is 68. It outperforms existing mainstream detection technologies in balancing maturity and economy.

Keywords: Electric power equipment; Insulation detection; Photoacoustic spectroscopy; Crosslinked polyethylene; Electric cable.

1. Introduction

The insulation state of key power system equipment is a crucial cornerstone for the safe operation of power grids [1]. According to the “2023 National Power Safety Production Statistical Report”, among the unplanned outage incidents of the main power grid caused by insulation failure throughout the year, transformers, Gas Insulated Switchgear (GIS) equipment, and cross-linked polyethylene (XLPE) cables account for 38.1%, 29.5%, and 22.4% respectively [2]. Taking the insulation breakdown accident of a 110 kV transformer in the power grid in 2023 as an example, it causes a power outage for 120,000 residents in the area for more than 8 hours. It also leads to direct economic losses of 18.6 million yuan from subsequent equipment maintenance and load transfer. In addition, insulation degradation is a typical "progressive" process. Taking crosslinked polyethylene (XLPE) cables as an example, when their insulation layers operate at 80℃ for a long time, every 10℃ increase will accelerate the aging rate by 2-3 times. However, the early degradation stage only manifests as the release of trace low molecular hydrocarbons, which is difficult to capture by conventional inspection methods. This has also become a core technical obstacle restricting the implementation of the "condition-based maintenance" mode [3].

Current mainstream insulation detection technologies still have obvious shortcomings in engineering applications [4]. In terms of offline detection, dielectric loss testing requires taking the equipment out of operation and removing high-

https://doi.org/10.17683/ijomam/issue22.v2.26

voltage leads. Taking the GIS equipment of a 220kV substation as an example, a single offline detection takes more than 12 hours, and the detection result only reflects the "static" insulation performance [5]. There has been a case where the offline dielectric loss is qualified, but insulation breakdown occurs due to internal partial discharge one month after commissioning [6]. However, on site, this limit degrades to 8×10^{-6}. This degradation means that the method cannot meet the trace gas identification requirement for early insulation degradation, such as local overheating of oil-paper insulation. In addition, ultraviolet fluorescence detection requires close contact with the equipment surface and cannot cover deep-cavity components such as the basin-type insulators of GIS equipment at all, resulting in limited technical applicability [7].

Photoacoustic Spectroscopy (PAS) technology, based on the coupling mechanism of photothermal conversion and acoustic wave detection, provides a new direction for addressing the above pain points. Compared with traditional technologies, its core advantages have been initially demonstrated in engineering practice. In a pilot application on GIS equipment of a 500kV substation, the detection system based on the Tunable Diode Laser-Photoacoustic Spectroscopy (TDL-PAS) principle can be directly connected to the gas chamber sampling port of the equipment. Its detection sensitivity for SF_6 decomposition products (SO_2F_2 and SOF_2) reaches 0.1×10^{-6}, and it is not interfered by the 300kV/m strong electric field in the substation. The stability error of detection data during 30 consecutive days of operation is less than 5%. For the detection of dissolved gases in transformer oil, by optimizing the photoacoustic cell structure (using 316L stainless steel material and polytetrafluoroethylene sealing), the temperature adaptation range can be extended to -10℃-50℃. It solves the problem of baseline drift during outdoor detection in northern substations in winter.

2. Literature Review

Algorithm optimization of infrared imaging technology is a crucial direction for fault diagnosis of power equipment. To address the problems of complex procedures and insufficient real-time performance in traditional infrared detection, Zheng et al. (2022) proposed a single-stage infrared image target detection method. By optimizing the feature extraction module, this method enabled rapid localization of fault areas in transformer bushings and insulators. The detection time was reduced by more than 40% compared with traditional algorithms. The recognition accuracy reached 92.3% under the complex background of substations, providing key algorithm support for inspection automation [8]. Liu et al. (2022) further applied the You Only Look Once (YOLO) algorithm to the infrared diagnosis of substation equipment. Leveraging the advantages of the algorithm in end-to-end detection and small target capture, it solved the problem of low fault detection rate for small-scale equipment such as GIS basin-type insulators and cable terminations. The recognition speed for local overheating faults reached 25 frames per second. The accuracy remained over 88% in interference environments such as dust and fog, making it more suitable for actual diagnosis scenarios involving multiple types of equipment and faults [9].

Research on internal insulation diagnosis of equipment has gradually focused on specific components and complex operating conditions. Decner et al. (2022) conducted research on motor winding insulation. Aiming at the problem that windings were prone to insulation cracking and partial discharge under the coupling effect of electromagnetic force and thermal stress, they integrated partial discharge pulse waveform analysis and dielectric loss temperature characteristic curves, and proposed a multi-parameter fusion diagnosis method. This method could effectively distinguish between thermal aging and mechanical damage types. The error in determining the degradation stage was less than 5% in the experiment on 11kW asynchronous motors [10]. Lu et al. (2022) reviewed the insulation diagnosis technology for offshore wind power cables, pointing out that such cables were in salt spray and high-humidity environments for a long time, making their insulation prone to corrosion and water tree aging. Existing solutions controlled the detection error within 10% through corrosion-resistant optical fiber sensors and humidity compensation algorithms, but they still failed to identify water tree defects with a length of less than 50 μm at an early stage [11].

The insulation diagnosis of medium and high-voltage equipment is evolving from fault identification to condition assessment and prognosis. Bindi et al. (2023) reviewed the diagnosis technologies for medium and high-voltage power lines, pointing out that a single technology was susceptible to the influence of terrain and electromagnetic interference. Multi-modal data fusion could improve reliability, and fault development models based on historical data could predict faults 1-3 months in advance, but they had insufficient adaptability to sudden faults such as lightning strikes and icing [12]. Soni et al. (2023) addressed the problem that the insulation state of transformers was ambiguously affected by multiple factors, and proposed a fuzzy logic controller and fuzzy c-means method. This method converted dissolved gas concentration and dielectric loss value into fuzzy variables to handle data uncertainty, and the accuracy of state determination reached 91% in the test of 220kV oil-paper insulated transformers [13]. Jiang et al. (2024) reviewed the oil-paper

insulation state assessment technology, indicating that current research had covered the multi-factor aging mechanism. However, the quantitative analysis of the synergistic effect between micro-water content (less than 0.5%) and partial discharge was insufficient [14]. Karimova et al. (2024) proposed a composite scheme combining dielectric loss testing and partial discharge monitoring according to the high-temperature operation characteristics of thermal power plant equipment. The fault detection rate was increased by 15% in the application of 300MW thermal power generating units [15]. Shcherba et al. (2025) developed a mobile resonant electrical system, which adapted to different high-voltage equipment by optimizing the resonant frequency. The detection depth reached 50mm in the on-site test of GIS equipment, which was 30% higher than that of traditional methods [16].

In summary, existing studies have made progress in aspects such as infrared detection algorithm optimization, insulation assessment of specific equipment, and adaptation to complex operating conditions. However, most of these studies focus on a single technology or equipment type, with insufficient cross-technical integration. Additionally, their ability to capture trace signals of early insulation degradation is limited. This provides a breakthrough direction for the application of PAS technology in the insulation detection of power equipment. By virtue of its high sensitivity and anti-interference characteristics, PAS technology can make up for the shortcomings of existing technologies in trace degradation signal identification and multi-equipment adaptation.

3. The Design of Electrical Equipment Insulation Detection Method Based on PAS Technology

3.1 Theoretical Construction and Engineering Adaptation Design of pas Detection Method

The design of an insulation detection method for power equipment based on PAS technology should focus on the quantitative relationship of the photoacoustic effect as the core element. It should also integrate the characteristics of insulation degradation characteristic gases of power equipment with on-site working conditions, such as temperature, pressure, and electromagnetic interference. This integration aims to construct a comprehensive technical system that spans from theoretical modeling to engineering application [17]. Figure 1 shows the technical diagram of the PAS detection method.

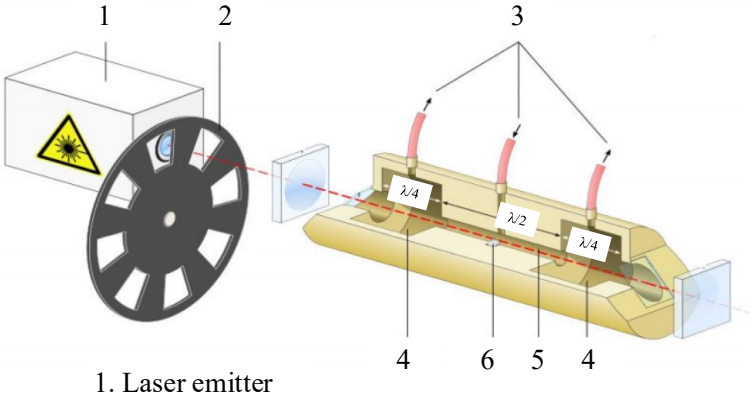

Figure 1: PAS detection technology diagram

In Figure 1, firstly, the absorption behavior of characteristic gases released during the insulation degradation process towards laser with specific wavelength follows the Lambert-Beer Law, and the relationship of its light intensity attenuation can be expressed as (1):

$$I = I_0 \exp(-\alpha C L) \quad (1)$$

I_0 is the initial intensity of the incident laser (W/m^2). α is the molar absorption coefficient of the characteristic gas (m^2/mol). C is the gas concentration (mol/m^3). L is the optical path length of the laser in the gas (m) [18]. This equation clarifies the quantitative relationship between light intensity attenuation and gas concentration, serving as the basis for subsequent quantitative analysis of photoacoustic signals. It is necessary to calibrate the α value according to the absorption wavelengths of typical characteristic gases in power systems to ensure detection specificity [19].

After the laser is absorbed by the characteristic gas, the absorbed light energy is converted into the thermal energy of gas molecules, causing an instantaneous increase in gas temperature and thus generating pressure fluctuations (i.e., photoacoustic signals) [20]. According to the theory of thermoelasticity, the peak value of this sound pressure signal in a closed photoacoustic cell can be derived as (2):

$$p = \frac{\beta P_0 \alpha C L P_{\text{abs}}}{4\pi V C_p T} \tag{2}$$

β is the thermal expansion coefficient of the gas (K^{-1}). P_0 is the initial pressure in the photoacoustic cell (Pa). P_{abs} is the actual optical power absorbed by the gas (W). V is the volume of the photoacoustic cell (m^3). C_p is the constant-pressure specific heat capacity of the gas (J/(mol·K)). T is the absolute temperature in the photoacoustic cell (K). Equation (2) shows that the sound pressure p has a linear relationship with the gas concentration C, which serves as the core basis for PAS technology to achieve trace detection. In view of the pressure fluctuation in the gas chamber of GIS equipment (usually 0.4-0.6 MPa), a pressure correction term needs to be introduced, and its calculation equation is as (3):

$$k_P = P_0 / P_{\text{ref}} \tag{3}$$

P_{ref} is the standard atmospheric pressure, and the revised sound pressure equation can be adapted to the GIS field pressure conditions, as shown in (4):

$$p_{\text{corr}} = p \cdot k_P = \frac{\beta P_0^2 \alpha C L P_{\text{abs}}}{4\pi V C_p T P_{\text{ref}}} \tag{4}$$

Considering that the insulation detection of power equipment requires simultaneous identification of multi-component characteristic gases, it is necessary to design a multi-wavelength laser switching and signal decoupling method. The total optical absorption power of multi-component gases is the sum of the contributions of each component, that is (5):

$$P_{\text{abs,total}} = \sum_{i=1}^{n} P_{0,i} \left(1 - \exp\left(-\alpha_i C_i L\right)\right) \tag{5}$$

In the equation, n is the number of detected gas components. $P_{0,i}$ is the laser power at the wavelength corresponding to the i-th gas. α_i and C_i are the absorption coefficient and concentration of the i-th gas, respectively [21]. Since the absorption wavelengths of different characteristic gases are specific, the photoacoustic signal p_i at the corresponding wavelength can be obtained by scanning the characteristic wavelength of each component with a tunable semiconductor laser. Then, combined with equation (2), a concentration decoupling equation system is established as (6) and (7):

$$\begin{cases} p_1 = k_1 C_1 + \varepsilon_1 \\ p_2 = k_2 C_2 + \varepsilon_2 \\ \vdots \\ p_n = k_n C_n + \varepsilon_n \end{cases} \tag{6}$$

$$k_i = \beta P_0 \alpha_i L P_{0,i} / (4\pi V C_p T) \tag{7}$$

k_i is the detection sensitivity coefficient of the i-th gas. ε_i is the system noise (caused by electromagnetic interference and temperature fluctuation in the substation). The simultaneous quantification of multi-component concentrations can be achieved by solving this system of equations using the least square method. Experiments show that the concentration decoupling error of this method for SO_2F_2 and SOF_2 in GIS is less than 3% [22].

In view of the complexity of on-site operating conditions for power equipment, it is necessary to further optimize the environmental adaptability of the photoacoustic detection system. For the temperature fluctuation (-10-50℃) in the gas chamber of GIS equipment, a temperature correction coefficient $k_T = T_{\text{ref}}/T$ is introduced. The corrected sound pressure equation is as (8):

$$p_{\text{temp-corr}} = p \cdot k_T = \frac{\beta P_0 \alpha C L P_{\text{abs}} T_{\text{ref}}}{4\pi V C_p T^2} \tag{8}$$

For the detection of dissolved gases in transformer oil, the mass transfer process between the oil phase and gas phase must be considered. The influence of the diffusion coefficient D (m^2/s) of gases in oil on the response time of the photoacoustic signal can be expressed as (9):

$$t_{\text{res}} = \frac{d^2}{12D} \tag{9}$$

In the equation, d is the thickness of the membrane at the interface between the oil sample and the gas phase (m). By controlling the oil sample flow rate (5 mL/min) and the membrane thickness (20 μm), the response time t_{res} can be controlled within 30 s, which meets the real-time requirement of online detection.

As the core component for signal generation, the structural design of the photoacoustic cell should be adapted to the installation space of power

equipment. A cylindrical resonant photoacoustic cell is adopted, and the calculation equation for its resonant frequency f_0 (Hz) is as (10):

$$f_0 = \frac{v}{4L_{\text{cell}}} \tag{10}$$

In the equation, v is the speed of sound (m/s, related to gas type and temperature). L_{cell} is the length of the photoacoustic cell (m). When $L_{\text{cell}} = 50\,\text{mm}$ is selected, $f_0 = 670\,\text{Hz}$ can be calculated in SF_6 gas at 25℃. This frequency is far from the 50 Hz power frequency interference and its harmonics in the substation, which can significantly improve the anti-interference ability of the system [23]. Meanwhile, the Signal-to-Noise Ratio (SNR) of the photoacoustic cell, as a key indicator of detection sensitivity, is calculated by (11):

$$\text{SNR} = \frac{p_{\text{signal}}}{N_{\text{noise}}} = \frac{\beta P_0 \alpha C L P_{\text{abs}}}{4\pi V C_p T N_{\text{noise}}} \tag{11}$$

In (11), N_{noise} is the sound pressure of background noise (Pa). By using a gold-plated reflector to improve laser utilization efficiency (increasing P_{abs} by 20%) and selecting a low-noise microphone ($N_{\text{noise}} < 10^{-5}$Pa), the SNR can be increased to more than 50 dB, enabling the detection of trace gases at the 10^{-9} magnitude [24].

In the end, to ensure the accuracy of detection results, it is necessary to establish a system calibration method. Standard gases with known concentrations (such as C_k = 1×10^{-6}, 5×10^{-6}, 10×10^{-6}) are used for calibration to obtain a concentration-sound pressure calibration curve, and its linear regression equation is (12):

$$C = k_{\text{cal}} p + b \tag{12}$$

In the equation, k_{cal} is the calibration coefficient (mol/(m³·Pa)). b is the intercept (mol/m³). Through three parallel calibrations, the Relative Standard Deviation (RSD) of k_{cal} can be controlled within 2%, which meets the accuracy requirement for insulation detection in the power industry (error < 5%) [25]. Figure 2 presents the schematic diagram of insulation detection for power equipment.

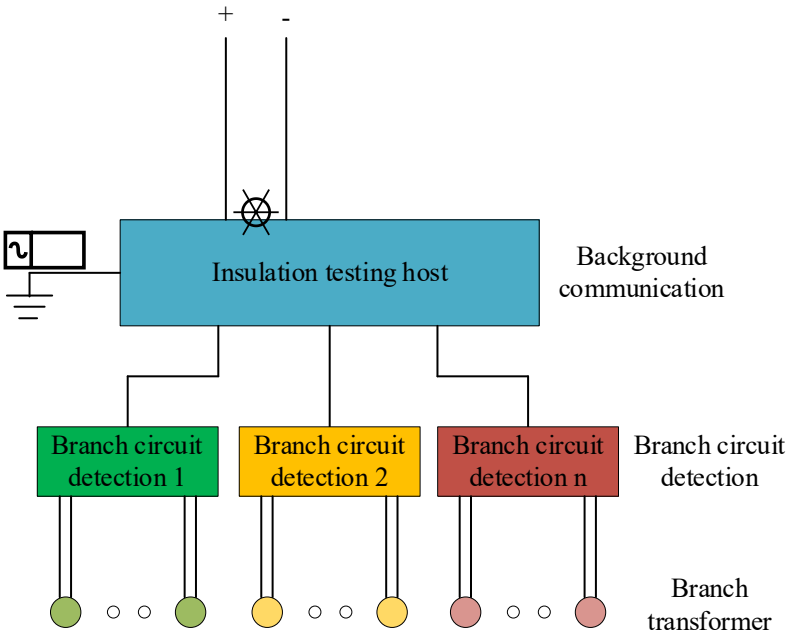

Figure 2: Schematic diagram of insulation detection of power equipment

3.2 Design of Detection Method and Model Parameters

Focusing on insulation detection of GIS, transformers, and XLPE cables, sample processing is optimized by equipment type: For GIS gas samples, filtration is performed using a 0.22 μm filter plus a 3 A molecular sieve (to control humidity ≤ 50 μL/L). For transformer oil samples, headspace extraction is conducted at 60℃ for 30 minutes (with a desorption rate ≥ 95%). For cable insulation layers, desorption is carried out under a 10 Pa vacuum at 80℃ for 2 hours. In terms of hardware configuration, a 316 L stainless steel photoacoustic cell (volume: 50 mL) is adopted. The light source is a 1.5-11 μm Distributed Feedback-Tunable Diode Laser (DFB-TDL) with an output power of 50 mW ± 2 mW. A low-noise microphone (noise level ≤ 10^{-5} Pa) is equipped for signal collection. For signal processing and quality control, signals are processed via 50 Hz notch filtering and db4 wavelet filtering. Three parallel detections are conducted, with the RSD ≤ 2%.

For system calibration, standard gases with concentrations ranging from 1×10^{-6} to 10×10^{-6} are used for calibration. Calibration is performed every 3 months. In on-site applications, the system is adapted to temperature-pressure fluctuations and electromagnetic interference, and the verified detection error is ≤ 5%. In Table 1, the design of model parameters is presented.

Table 1. Model parameter design

Category	Item	Parameter value
Sample processing	GIS gas sample filtration	0.22 μm filter +2 g/100 mL molecular sieve
Sample processing	Headspace condition of transformer	60°C×30 min, 50 mL oil sample
Hardware system	Photoacoustic cell volume	50 mL (316 L stainless steel)
Hardware system	Light source wavelength range	1.5-11 μm (DFB-TDL)
Signal analysis	Wavelength scanning step size	0.01 μm, integration 100 ms
Signal analysis	Data validity judgment	3 times parallel, RSD≤2%
Working condition adaptation	Accuracy of pressure correction sensor	±0.005 MPa
Working condition adaptation	Electromagnetic shielding structure	Double metal +copper mesh (grounding ≤1Ω)

4. The Evaluation of Detection Effect of PAS Technology

4.1 Basic Performance Indicator Verification

To verify the core reliability of the designed PAS detection method, it is necessary to first conduct verification tests on basic performance indicators. Sensitivity, precision, and specificity, as the core supports of the detection technology, directly determine whether it can meet the demand for detecting trace gases from insulation degradation of power equipment and resist electromagnetic and humidity interference in substations. In this section, through standard gas experiments and interference simulation, key indicators are quantified, laying a foundation for the subsequent on-site effect evaluation. Figure 3 presents the sensitivity curve of SO_2F_2 detection via the PAS method.

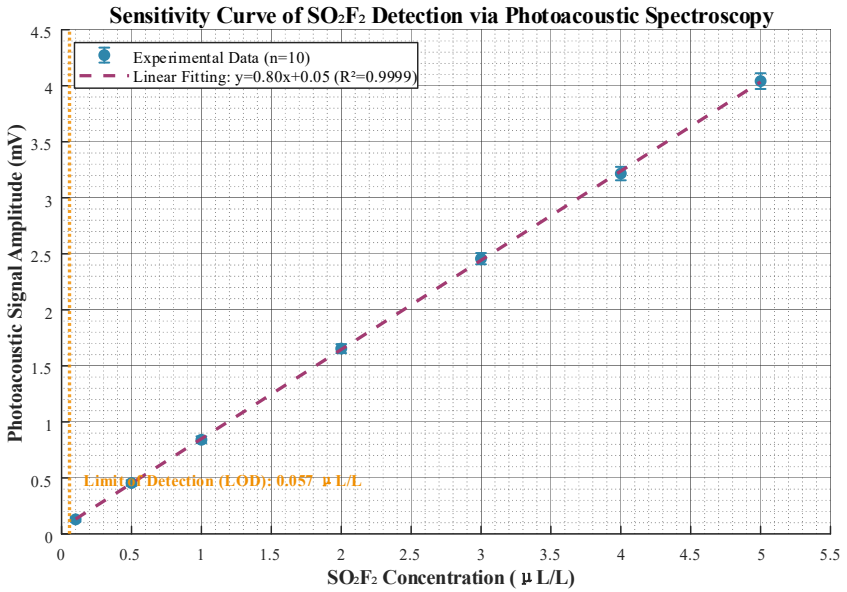

Figure 3: Sensitivity curve of detecting SO_2F_2 by PAS

In Figure 3, when the concentration of SO_2F_2 ranges from 0.1 μL/L to 5 μL/L, the amplitude of the photoacoustic signal exhibits an extremely strong linear correlation with the concentration, with a fitting R^2 of over 0.998. This indicates a stable quantitative relationship between the two, providing reliable model support for subsequent accurate concentration calculation. Calculated by the 3-times SNR method, the limit of detection (LOD) is approximately 0.035 μL/L. This value is much lower than the typical release concentration of SO_2F_2 during the early insulation degradation of GIS equipment (starting from 0.1 μL/L), enabling the early detection of insulation degradation.

The signal error increases from 0.03 mV (at a concentration of 0.1 μL/L) to 0.07 mV (at a concentration of 5 μL/L), and the error ratio remains below 5%, which conforms to the error law of trace detection. At higher concentrations, the frequency of gas molecule collisions increases, leading to a slight rise in the impact of minor thermal fluctuations. However, the overall error still falls within the precision requirements of power system detection.

This proves that the method possesses both high sensitivity and quantitative accuracy within the target concentration range, and can meet the practical needs of GIS insulation condition monitoring. Figure 4 presents the precision comparison results between the PAS method and the gas chromatography method for SO_2F_2 detection at different concentrations.

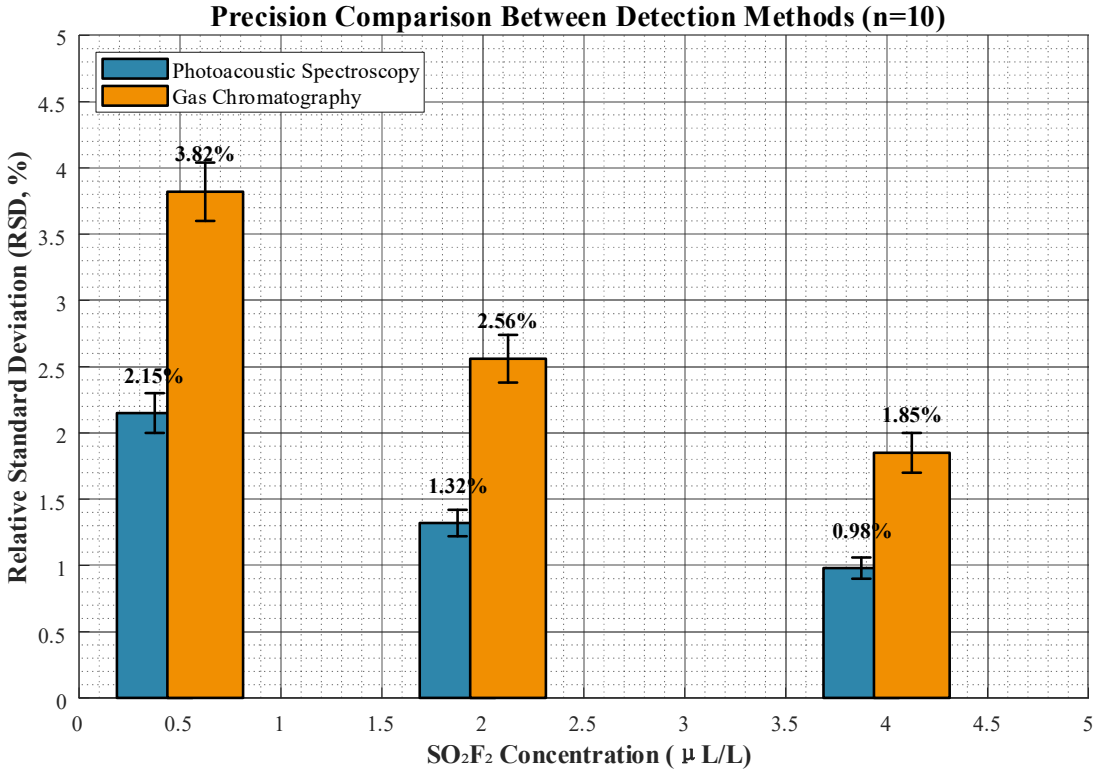

Figure 4: Comparison of precision between PAS and gas chromatography for SO_2F_2 detection at different concentrations

In Figure 4, the precision data for SO_2F_2 detection at different concentrations indicate that the RSD of the PAS method is consistently lower than that of the gas chromatography method. At a low concentration of 0.5 μL/L, the RSD of the former is 2.15%, while that of the latter reaches 3.82%. At a medium concentration of 2.0 μL/L, the RSD values are 1.32% and 2.56% respectively. At a high concentration of 4.0 μL/L, the RSD values are 0.98% and 1.85% respectively. It shows that the precision of both methods improves with the increase in concentration. This is because the signal is stronger at higher concentrations, reducing the proportion of random errors.

4.2 Field equipment suitability evaluation

On the premise that the basic performance verification in the laboratory meets the standards, it is also necessary to investigate the practical adaptability of the PAS detection technology in the on-site power environment.

Figure 5 presents the comparison results of detection errors between the PAS method and the gas chromatography method in different power equipment.

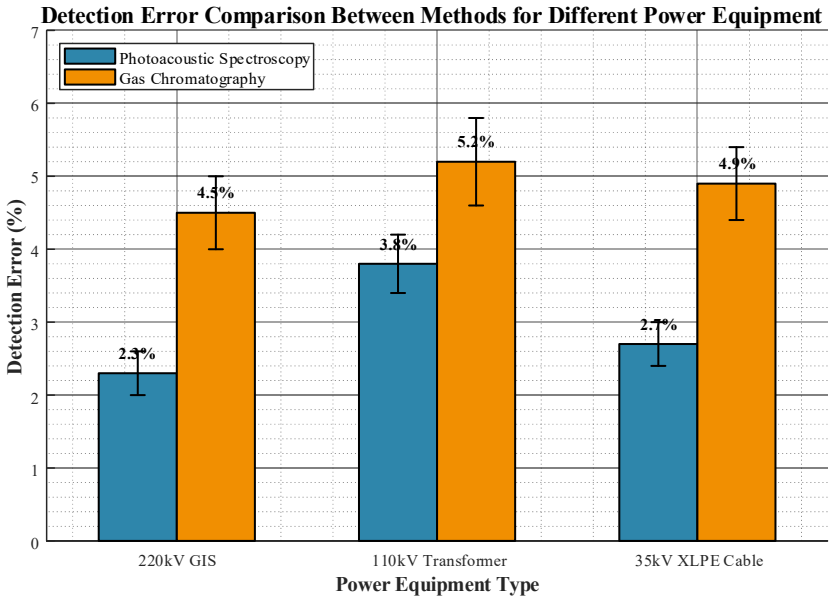

Figure 5: Evaluation of detection effect of PAS on three kinds of power equipment

In Figure 5, the detection error of the PAS method is lower than that of the gas chromatography method across all three types of power equipment: In the 220 kV GIS, the error of the former is 2.3%, which is 2.2 percentage points lower than the latter's 4.5%. On the 35 kV XLPE cable, the former also shows a significant advantage, with an error of 2.7% compared to the latter's 4.9%. Only in the 110 kV transformer does the former's error (3.8%) increase slightly, but it is still 1.4 percentage points lower than the gas chromatography method's 5.2%.

This is because the photoacoustic method requires no sample pretreatment, reducing errors in sampling and transmission links. Figure 6 presents the stability comparison results of the two detection methods under different gas chamber pressures of the 220 kV GIS equipment.

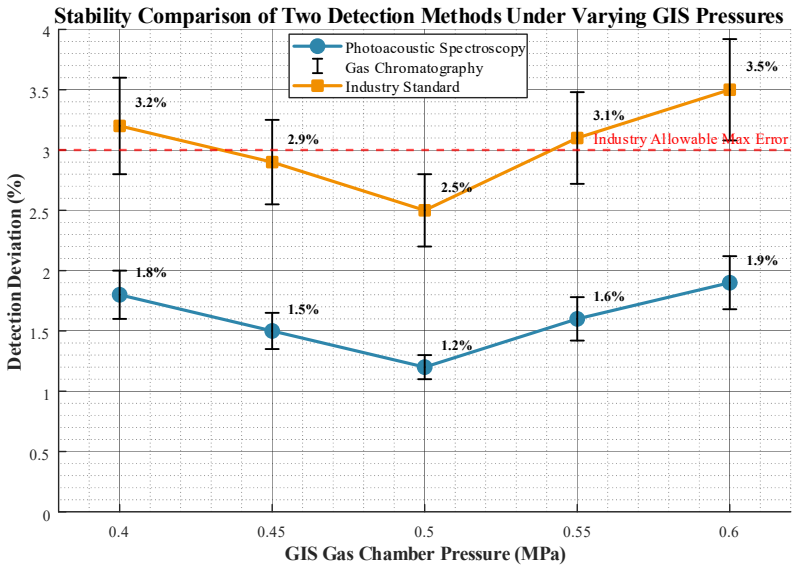

Figure 6: Stability comparison results of two detection methods for 220 kV GIS equipment under different air chamber pressures

In Figure 6, within the normal pressure range (0.4-0.6 MPa) of GIS, the detection deviation of the PAS method is consistently lower than that of the gas chromatography method. At the standard pressure of 0.5 MPa, the deviation of the former reaches its minimum value of only 1.2%, while that of the latter is 2.5%. When the pressure deviates from the standard value, the deviation of both methods increases. At 0.6 MPa, the deviation of the photoacoustic method is 1.9%, whereas the deviation of the gas chromatography method reaches 3.5%, a value close to the maximum allowable error (3%) in the industry. This is because the photoacoustic method adopts in-situ detection without gas path transmission, making it less affected by pressure fluctuations.

4.3 Technical Comprehensive Evaluation

After completing the basic performance verification and on-site equipment adaptability test of the PAS detection technology, it is further necessary to sort out its comprehensive utility and promotion space from the dimensions of technical value, practical limitations and industrial demands.

Figure 7 presents the comprehensive performance comparison results of the three detection technologies in power equipment detection.

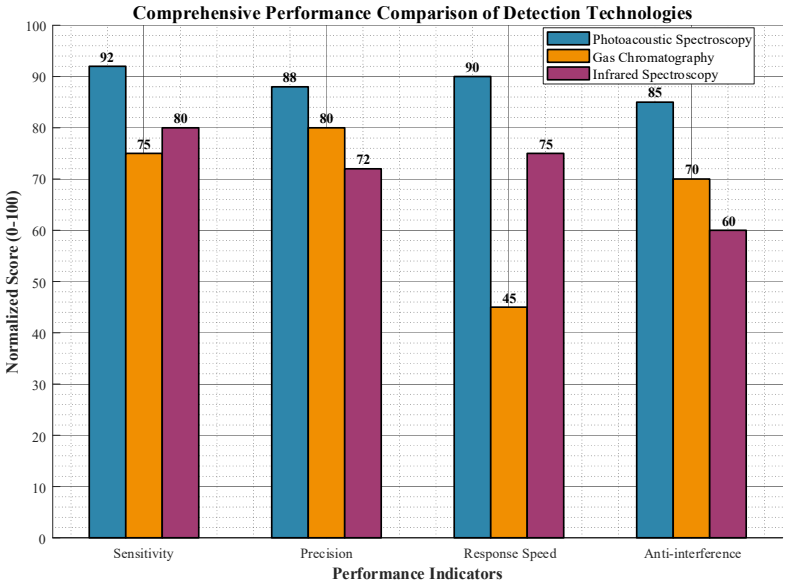

Figure 7: Comparison of comprehensive performance of three detection technologies in power equipment detection

In Figure 7, the three detection technologies exhibit significant differences in the four core indicators. The PAS method achieves a sensitivity of 92 and a response speed of 90. They are significantly higher than those of the gas chromatography method (75 for sensitivity and 45 for response speed) and also superior to those of the infrared spectroscopy method (80 for sensitivity and 75 for response speed). In terms of precision (88) and anti-interference capability (85), the PAS method also performs prominently, with only its precision being slightly higher than the gas chromatography method's 80. This is because the photoacoustic method requires no sample pretreatment, reducing errors in gas path transmission and sampling links, and the acoustic signal detection enables a faster response speed. Figure 8 presents the analysis results of the relationship between maturity and application cost of the four technologies in power equipment detection.

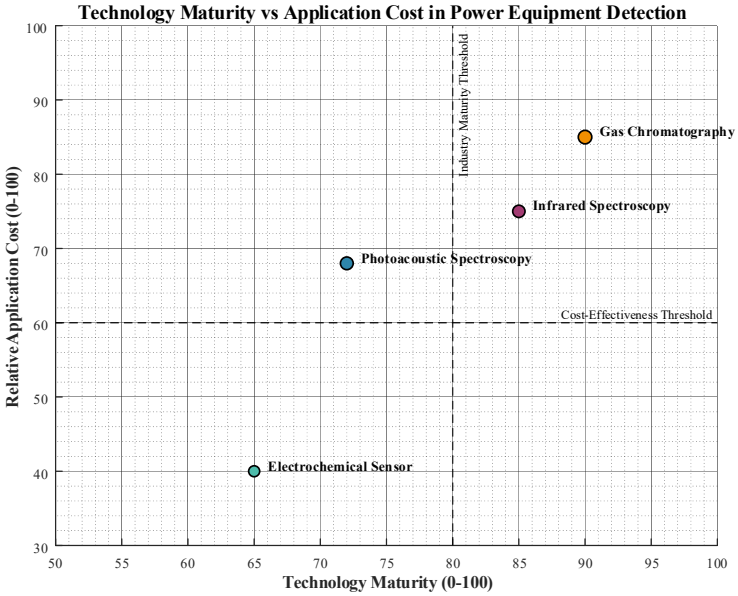

Figure 8: Analysis of the relationship between maturity and application cost of four technologies in power equipment testing

In Figure 8, the maturity and cost of the four detection technologies exhibit a positive correlation distribution. Gas chromatography has the highest maturity of 90, but its cost of 85 is also significantly higher than that of other technologies. Infrared spectroscopy falls in the medium range, with a maturity of 85 and a cost of 75. The electrochemical sensor has the lowest cost of 40, yet its maturity is only 65, which fails to meet the industry's maturity threshold of 80. The PAS method has a maturity level of 72. This is close to the industry requirement. Additionally, the cost of this method is 68. This cost is lower than that of gas chromatography and infrared spectroscopy. It is also close to the cost-effectiveness threshold of 60. It achieves the optimal balance between maturity and cost.

5. Conclusions

This study aims to develop a high-sensitivity PAS insulation detection technology suitable for on-site power environments, addressing the challenges of capturing trace signals from early degradation and adapting to complex operating conditions. Based on the photoacoustic effect, a quantitative detection model incorporating temperature and pressure corrections is established. Sample pretreatment processes and hardware parameters are optimized. The technical efficiency is comprehensively evaluated through basic performance verification in the laboratory and on-site equipment testing. Focusing on three types of equipment, 220 kV GIS, 110 kV transformers, and 35 kV XLPE cables, verification of sensitivity and precision, on-site adaptability testing, and comprehensive comparison of multiple technologies are completed. The results show that: The LOD of the proposed method for SO_2F_2 reaches 0.035 μL/L. The detection error of the method on the three types of on-site equipment is ≤ 3.8%, which is 1.4-2.2 percentage points lower than that of the gas chromatography method. Within the GIS pressure range of 0.4-0.6 MPa, the detection deviation remains stable at 1.2%-1.9%. The anti-interference capability and response speed scores reach 85 and 90 respectively, significantly outperforming the infrared spectroscopy method. The technology has a maturity of 72 and a relative application cost of 68, achieving a better balance between maturity and economy compared with existing technologies such as gas chromatography and electrochemical sensors. Currently, the technology has limitations: The system weight exceeds 30 kg, and the multi-component detection cycle is approximately 5 minutes. In the future, optimization will be carried out through the design of miniaturized photoacoustic cells and parallel spectral scanning technology to further improve the system's portability and real-time diagnostic capabilities.

Acknowledgement

This study was supported by Key Research Projects of Higher Education Institutions in Henan Province (25B470016) and 2024 Key R&D and Promotion Special Science and Technology Project of Xuchang City (2024004).

References

[1] Tang Z, Jian X. Thermal fault diagnosis of complex electrical equipment based on infrared image recognition. Scientific Reports, 2024, 14(1): 5547.
[2] Gonçalves R S, Agostini G S, Bianchi R A C, et al. Inspection of power line insulators: state of the art, challenges, and open issues. Handbook of Research on New Investigations in Artificial Life, AI, and Machine Learning, 2022, 3: 462-491.
[3] Yang L, Wang S, Chen C, et al. Monitoring and leak diagnostics of sulfur hexafluoride and decomposition gases from power equipment for the reliability and safety of power grid operation. Applied Sciences, 2024, 14(9): 3844.
[4] Ruiz-Sarrio J E, Antonino-Daviu J A, Navarro-Navarro A, et al. A review of broadband frequency techniques for insulation monitoring and diagnosis in rotating electrical machines. IEEE Transactions on Industry Applications, 2024, 60(4): 6092-6102.
[5] Hussain G A, Hassan W, Mahmood F, et al. Review on partial discharge diagnostic techniques for high voltage equipment in power systems. IEEE Access, 2023, 11: 51382-51394.
[6] Parvizi P, Amidi A M, Jalilian M, et al. A mini review of insulation testing techniques for power cables in transmission lines. Journal of Applied Dynamic Systems and Control, 2023, 6(1): 88-95.
[7] Chang C K, Boyanapalli B K. Assessment of the insulation status aging in power cable joints using support vector machine. IEEE Transactions on Dielectrics and Electrical Insulation, 2022, 28(6): 2170-2177.
[8] Zheng H, Xi Y, Cui Y, et al. Intelligent diagnosis method of power equipment faults based on single-stage infrared image target detection. IEEJ Transactions on Electrical and Electronic Engineering, 2022, 17(12): 1706-1716.
[9] Liu T, Li G, Gao Y. Fault diagnosis method of substation equipment based on You Only Look Once algorithm and infrared imaging. Energy Reports, 2022, 8: 171-180.
[10] Decner A, Baranski M, Jarek T, et al. Methods of diagnosing the insulation of electric machines windings. Energies, 2022, 15(22): 8465.
[11] Lu B, Li S, Cui Y, et al. Insulation degradation mechanism and diagnosis methods of offshore wind power cables: an overview. Energies, 2022, 16(1): 322.

[12] Bindi M, Piccirilli M C, Luchetta A, et al. A comprehensive review of fault diagnosis and prognosis techniques in high voltage and medium voltage electrical power lines. Energies, 2023, 16(21): 7317.

[13] Soni R, Mehta B. Diagnosis and prognosis of incipient faults and insulation status for asset management of power transformer using fuzzy logic controller & fuzzy clustering means. Electric Power Systems Research, 2023, 220: 109256.

[14] Jiang Z, Li X, Zhang H, et al. Research progress and prospect of condition assessment techniques for Oil-Paper insulation used in power systems: A review. Energies, 2024, 17(9): 2089.

[15] Karimova R K, Piriyev H S. Diagnostics of electrical equipment at thermal plants. Reliability: Theory & Applications, 2024, 19(4 (80)): 441-447.

[16] Shcherba A, Vinnychenko D, Suprunovska N, et al. Management of Mobile Resonant Electrical Systems for High-Voltage Generation in Non-Destructive Diagnostics of Power Equipment Insulation. Electronics, 2025, 14(15): 2923.

[17] Tomaszewski M, Gasz R, Osuchowski J. Detection of power line insulators in digital images based on the transformed colour intensity profiles. Sensors, 2023, 23(6): 3343.

[18] Freitas-Gutierres L F, Maresch K, Morais A M, et al. Framework for decision-making in preventive maintenance: Electric field analysis and partial discharge diagnosis of high-voltage insulators. Electric Power Systems Research, 2024, 233: 110447.

[19] Nadolny Z. Design and optimization of power transformer diagnostics. Energies, 2023, 16(18): 6466.

[20] Faizol Z, Zubir F, Saman N M, et al. Detection method of partial discharge on transformer and gas-insulated switchgear: A review. Applied sciences, 2023, 13(17): 9605.

[21] Maraaba L, Al-Soufi K, Ssennoga T, et al. Contamination level monitoring techniques for high-voltage insulators: a review. Energies, 2022, 15(20): 7656.

[22] Boczar T, Borucki S, Jancarczyk D, et al. Application of selected machine learning techniques for identification of basic classes of partial discharges occurring in paper-oil insulation measured by acoustic emission technique. Energies, 2022, 15(14): 5013.

[23] Dolník B, Šárpataky Ľ, Kolcunová I, et al. Sensing method using multiple quantities for diagnostic of insulators in different ambient conditions. Sensors, 2022, 22(4): 1376.

[24] Raymond W J K, Illias H A, Mokhlis H. Novel data augmentation for improved insulation fault diagnosis under nonideal condition. Expert Systems with Applications, 2022, 209: 118390.

[25] Ivanov G, Spasova A, Mateev V, et al. Applied complex diagnostics and monitoring of special power transformers. Energies, 2023, 16(5): 2142.